

Mesenteric abnormalities play an important role in grading intestinal fibrosis in patients with Crohn's disease: a computed tomography and clinical marker-based nomogram

Jixin Meng*¹, Yitao Mao*, Jie Zhou*, Zhao Chen, Siyun Huang, Yangdi Wang, Li Huang, Ruonan Zhang, Xiaodi Shen, Wen Lv, Juxiong Xiao, Ziyin Ye, Zhihui Chen, Ren Mao, Canhui Sun, Ziping Li, Shi-Ting Feng, Shaochun Lin and Xuehua Li²

Abstract

Background: While the grading of intestinal fibrosis is closely related to the therapeutic strategy of patients with Crohn's disease (CD), it has not yet been well resolved. Mesenteric abnormalities are inextricably linked to intestinal fibrosis.

Objectives: We aimed to establish an optimal model for assessing intestinal fibrosis using computed tomography enterography (CTE) and clinical markers.

Design: A total of 174 patients with CD between January 2014 and June 2020 were included in this retrospective multicentre study.

Methods: All patients underwent CTE within 3 months prior to surgery. Intestinal fibrosis was pathologically scored as non-mild or moderate-to-severe. Selected imaging of the intestinal walls and mesentery and/or clinical factors were used to develop the diagnostic models. The area under the receiver operating characteristic curve (AUC) analysis was used to evaluate the discrimination performance of the models. A decision curve analysis was performed to evaluate the clinical usefulness of the models.

Results: One-, two-, and three-variable models were identified as possible diagnostic models. Model 1 [mesenteric creeping fat index (MCFI)], Model 2 (mesenteric oedema and MCFI), and Model 3 (mesenteric oedema, MCFI, and disease duration) were established. The AUCs of Model 1 in training and test cohorts 1 and 2 were 0.799, 0.859, and 0.693, respectively; Model 2 was 0.851, 0.833, and 0.757, respectively; and Model 3 was 0.832, 0.821, and 0.850, respectively. We did not observe any significant difference in diagnostic performance between the training and total test cohorts in any model (all $p > 0.05$). The decision curves showed that Model 3 had the highest net clinical benefit in test cohort 2. The nomogram of this optimal model was constructed by considering the favourable and robust performance of Model 3.

Conclusion: A nomogram integrating mesenteric abnormalities on CTE with a clinical marker was optimal for differentiating between non-mild and moderate-to-severe fibrosis in patients with CD.

Keywords: computed tomography enterography, Crohn's disease, fibrosis, mesentery, nomogram

Received: 1 April 2022; revised manuscript accepted: 26 July 2022.

Ther Adv Gastroenterol

2022, Vol. 15: 1–13

DOI: 10.1177/
17562848221122504

© The Author(s), 2022.
Article reuse guidelines:
sagepub.com/journals-
permissions

Correspondence to:

Xuehua Li
Department of Radiology,
The First Affiliated
Hospital, Sun Yat-sen
University, 58 Zhongshan II
Road, Guangzhou 510080,
People's Republic of
China.

lxueh@mail.sysu.edu.cn

Shaochun Lin
Department of Radiology,
The First Affiliated
Hospital, Sun Yat-sen
University, 58 Zhongshan II
Road, Guangzhou 510080,
People's Republic of China
lschun@mail.sysu.edu.cn

Jixin Meng
Siyun Huang
Yangdi Wang
Li Huang
Ruonan Zhang
Xiaodi Shen
Wen Lv
Canhui Sun
Ziping Li
Shi-Ting Feng
Department of Radiology,
The First Affiliated
Hospital, Sun Yat-sen
University, Guangzhou,
People's Republic of China

Yitao Mao
Juxiong Xiao
Department of Radiology,
Xiangya Hospital,
Central South University,
Changsha, Hunan,
People's Republic of China

Jie Zhou
Department of Radiology,
The Sixth Affiliated
Hospital, Sun Yat-sen
University, Guangzhou,
People's Republic of China

Zhao Chen
Department of Medical
Imaging Center, Nan Fang
Hospital, Southern Medical
University, Guangzhou,
People's Republic of China

Ziyin Ye

Department of Pathology, The First Affiliated Hospital, Sun Yat-sen University, Guangzhou, People's Republic of China

Zhihui Chen

Department of Gastrointestinal and Pancreatic Surgery, The First Affiliated Hospital, Sun Yat-sen University, Guangzhou, People's Republic of China

Ren Mao

Department of Gastroenterology, The First Affiliated Hospital, Sun Yat-sen University, Guangzhou, People's Republic of China

Department of Gastroenterology, Hepatology and Nutrition, Digestive Diseases and Surgery Institute, Cleveland Clinic, Cleveland, Ohio, USA

*These authors contributed equally.

Introduction

As an important complication of Crohn's disease (CD), moderate-to-severe fibrosis-predominant intestinal stricture contributes to refractory intestinal obstruction, which often requires surgical treatment¹ whereas the obstruction symptoms caused by non-mild fibrosis-dominated intestinal stenosis can often be relieved by medical treatment.^{2,3} Hence, the ability to distinguish the degree of strictured intestinal fibrosis to guide the individualized treatment of patients with CD in clinical practice is vitally important and urgent.

Computed tomography enterography (CTE) is one of the most common and effective tools for detecting and monitoring bowel disease in patients with CD.⁴ However, previous studies have suggested that the conventional CTE findings analysed by radiologists had no correlation with intestinal fibrosis, indicating the inefficiency of CTE for evaluating intestinal fibrosis.⁵ The reason for this disappointing conclusion may be that most previous studies only focused on the characteristics of the diseased intestine and paid less attention to the potential value of the mesentery.

Creeping fat (CF) is an expansion of the mesenteric adipose tissue that wraps around the mesenteric side of the affected intestinal walls in CD; CF was first proposed in 1932 but was not taken seriously as a trait of CD until recently.^{6,7} In recent years, an increasing number of studies have shown that CF is closely related to intestinal fibrotic stenosis in CD at the gross level.⁷⁻⁹ In general, the most intuitive way to observe the morphology and extent of CF entanglement around a diseased intestine is through surgery and pathology. Our recent research showed that the novel mesenteric creeping fat index (MCFI) could accurately characterize the range of CF wrapped around the intestine and that the CF represented by MCFI was significantly positively correlated with collagen fibre deposition and smooth muscle hyperplasia/hypertrophy within the intestinal walls in CD patients.¹⁰ However, intestinal fibrosis is a complex pathological process caused by multiple factors, and the effectiveness of MCFI as a single parameter for identifying intestinal fibrosis remains limited. This issue may be better addressed by selecting efficient factors to construct a multiparameter diagnostic model from various candidate factors, such as CTE signs

in the intestinal tract and mesentery, as well as clinical markers.

This study compared the diagnostic efficacy of three models that included mesenteric CTE findings and/or clinical indicators in the evaluation of intestinal fibrosis, with the aim of developing an optimal diagnostic nomogram for an intuitive and quantitative evaluation of the degree of intestinal fibrosis in patients with CD.

Methods

Patients and data cohorts

A total of 174 consecutive patients with CD underwent surgery between January 2014 and June 2020 at Centre 1 (the First Affiliated Hospital of Sun Yat-sen University), Centre 2 (the Sixth Affiliated Hospital of Sun Yat-sen University), and Centre 3 (Nanfeng Hospital of Southern Medical University). The inclusion criteria for patients were as follows: (1) patients diagnosed with CD by clinical examination, radiology, endoscopy, and pathology; (2) patients who underwent CTE examination within 3 months before surgery; (3) patients' intestinal segments corresponded to a matching location on surgical specimens with available CTE images; and (4) patients had complete clinical, laboratory, pathological, and imaging data. The exclusion criteria were as follows: (1) patients with a history of enterectomy, (2) patients with an unclear display of mesenteric fat tissue adjacent to the diseased bowel walls due to penetrating lesions, or (3) patients who underwent emergency CT examination without enhancement. The surgical indications included refractory intestinal obstructions, fistulas, abscesses, or bowel perforations.

Of the 214 patients who met the inclusion criteria, 40 were excluded, resulting in a final enrolment of 174 patients (Figure 1). The first 91 patients in Centre 1 were assigned to the training cohort, while the other 30 patients in Centre 1 were assigned to the test cohort 1; 35 patients in Centre 2 and 18 patients in Centre 3 were assigned to the external test cohort 2.

Clinical markers, including age, sex, disease duration (months), time interval between CTE and

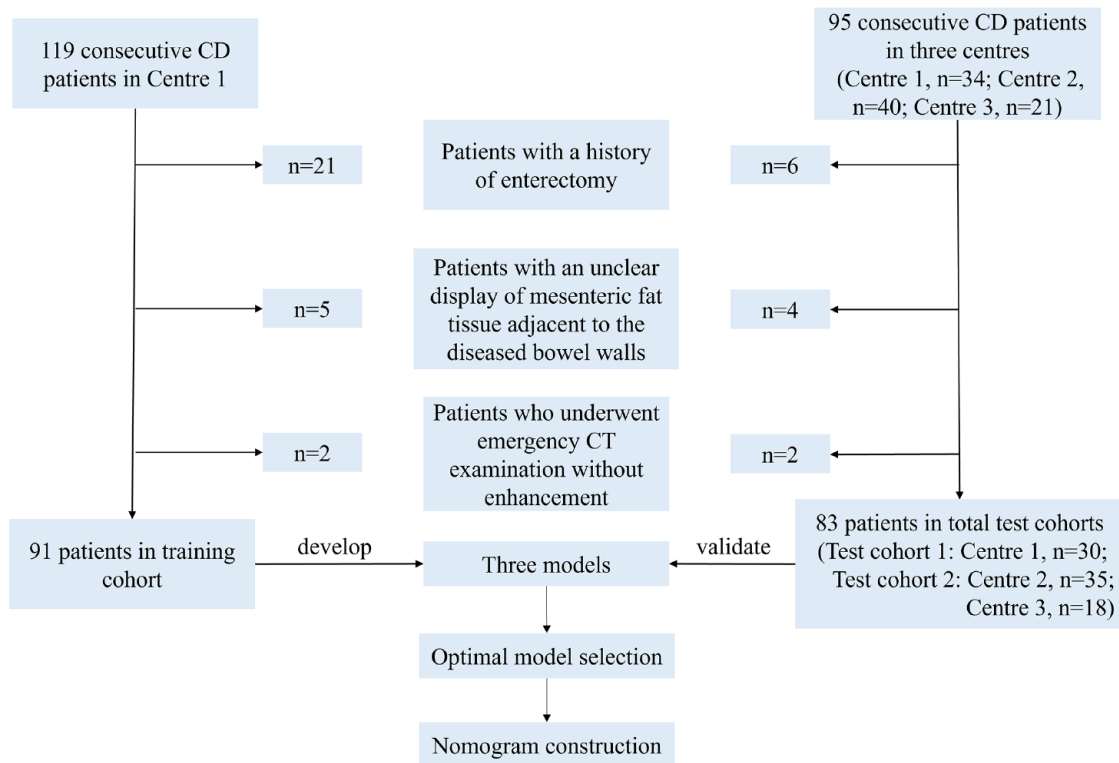


Figure 1. Patient enrolment flowchart.
CD, Crohn's disease; CT, computed tomography.

surgery (days), history of smoking, and preoperative use of drugs were collected from the hospital information system.

Location matching of the affected intestinal wall between CTE and the gross specimen

We adopted a region-to-region positioning approach between the CTE and gross specimen.^{10–12} Location matching was performed by a radiologist with 29 years of imaging experience (C.S.) in the imaging diagnosis of gastrointestinal diseases and a gastrointestinal surgeon (Z.C.) with 10 years of CD bowel resection experience, referring to data (e.g. location, morphology, and length of target bowel segment) extracted from the surgical or pathology report for the retrospective collection cases, or based on the anatomical landmarks (e.g. the ileocecal valve, appendix) and lesion characteristics (e.g. intestinal stenosis, fistulas, and abscesses) observed in the operating room for prospective collection cases, according to our previous research methods.¹³

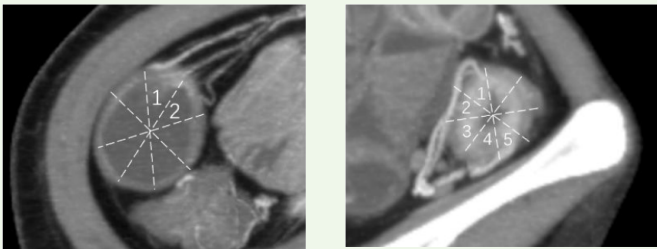
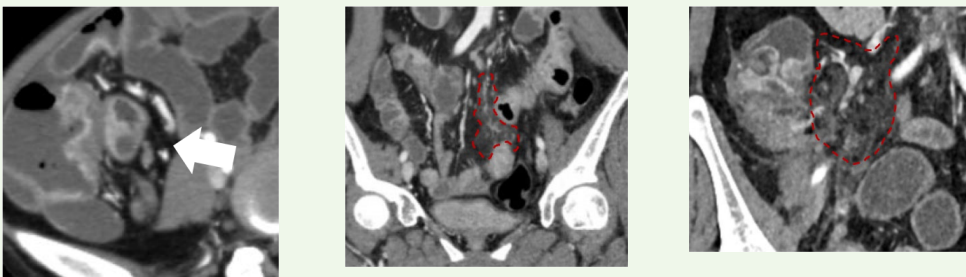
Pathological score of intestinal fibrosis

The full-thickness intestinal walls where the lumen was the narrowest and/or the intestinal wall was thickest were taken from each patient, fixed in formalin solution, embedded in paraffin, and cut into 4 µm-thick slices, and then Masson trichrome staining was used to determine the fibrosis score. A pathologist (Z.Y.) with 12 years' experience in the pathological diagnosis of gastrointestinal diseases, blinded to the patient's clinical data, laboratory examination, or CTE data, performed semiquantitative fibrosis scoring scaled between 0 and 4 points (as shown in Supplemental Table 1) according to the most obvious lesions on slides.⁵ Scores of 0–2 were classified as non-mild fibrosis, and 3 and 4 were considered moderate-to-severe fibrosis.¹³

CTE analysis

All patients underwent a preoperative CTE examination (CTE protocols are shown in the Supplemental Materials). The CTE findings of the affected gut were evaluated by the radiologist

Table 1. Definition, images and grading of the selected mesenteric CTE findings.

CTE findings	Definition	Images and grading
<i>Mesenteric features</i>		
MCFI	An imaging index that indirectly describes the degree of CF wrapping around the gut using the mesenteric vessels and scoring from 1 to 8.	 <p style="text-align: center;">Score 2 Score 5</p>
Mesenteric oedema	A general increase in the attenuation of mesenteric fat.	 <p style="text-align: center;">None Mild Moderate-to-severe</p>
In each image, white arrows or red lines indicate CTE findings. CF, creeping fat; CTE, computed tomography enterography; MCFI, mesenteric creeping fat index.		

(J.M.) who was blinded to the pathological fibrosis scores and had 4 years of experience in diagnostic imaging of CD using RadiAnt DICOM Viewer (Version 2020.2.1, Medixant company, Poznan, Poland).

Intestinal stricture on CTE was defined as a thickening of the affected intestinal wall of more than a 25% and a narrowing of the lumen of less than 50% compared with the adjacent well-filled normal bowel.³ CTE findings included intestinal and mesenteric features (Table 1 and Supplemental Table 2).

Intestinal features. Enhancement patterns of the intestinal walls from the arterial to venous phase were classified into three types: continuous layered enhancement, from layered to transmural enhancement, and continuous transmural enhancement. The thickness of the thickest bowel wall and its luminal diameter were measured using a standard cross-section of the affected

segments. Prestenotic dilatation was defined as the proximal lumen diameter of the narrow bowel greater than 3 cm.

Mesenteric features. The MCFI was reconstructed and calculated for the target bowel segments using the approach reported in our previous study.¹⁰ First, the enhanced CTE images were reconstructed using multiplanar reconstruction, and the cross-position lines were adjusted parallel and perpendicular to the long axis of the target bowel on the RadiAnt DICOM Viewer. Then, maximum intensity projection was performed to evaluate the range of mesenteric vessels covering the intestine in the standard axial position of the target intestine. A circle was made along the external margin of the intestinal wall, centred on the midpoint of the intestinal lumen, and divided into eight equal parts according to the central angle. The number of mesenteric vessels covering eight equal parts comprised the MCFI score, which ranged from 1 to 8 points.

The fibrofatty proliferation score was evaluated according to the degree of mesenteric fat increase around the affected intestine and the degree of displacement of the adjacent intestine. A score of 0–2 points corresponded to none, mild, and moderate-to-severe, respectively.^{10,14}

The comb sign was defined as the dilation and curvature of the mesenteric vessels of the diseased bowel, which were arranged in a comb shape.¹⁵ Absence of the comb sign was recorded as a score of 0. A mesenteric vessel diameter increase of not more than two times the normal was considered mild (score 1), and that more than two times the normal was considered moderate-to-severe (score 2).¹⁴

Mesenteric effusion was defined as a collection of free mesenteric fluid.¹⁶ The absence of mesenteric effusion was recorded as a score of 0. The largest vertical distance from the mesenteric effusion to the mesenteric side of the affected intestinal walls less than 15 mm was mild (score 1) and that longer than 15 mm was moderate-to-severe (score 2).¹⁷

Mesenteric oedema was defined as a general increase in the attenuation of mesenteric fat.¹⁶ The severity of mesenteric oedema was graded as none (score 0) if absent, mild (score 1) if there was a minimal wispy increase in the attenuation of mesenteric adipose tissue, or moderate-to-severe (score 2) if the increase in attenuation was more than minimal.¹⁷

Increased peri-intestinal lymph nodes were also considered a finding of abnormal mesentery.¹⁸ A finding of more than three peri-intestinal lymph nodes was considered positive (score 1); otherwise, it was considered negative (score 0).

Based on the pixel number of CTE images, the visceral to subcutaneous fat area ratio at the levels of the third lumbar (L3) and fourth lumbar (L4) vertebral bodies was automatically measured and calculated using fat assessment software at the Vitrea workstation (Canon Medical System, Otawara, Japan), which was operated by a radiologist (L.H.) with 8 years of experience in abdominal imaging diagnosis who was blinded to the pathological information.¹⁹ In addition, intestinal fistulas and perienteric abscesses were evaluated.

In order to test the intra-/interobserver consistencies of some subjective mesenteric signs, 50

patients were randomly selected from the total test cohort for re-evaluation by two radiologists (J.M. and S.H.) at a time interval greater than 3 months.

Variable selection and the development of diagnostic models in the training cohort

There were 18 pre-specified imaging and clinical variables in our dataset; one of them (enhancement pattern) was a disorderly classified variable, which needed to be expanded to three dummy variables. Thus, 20 variables were included in this dataset.

For the training cohort, the sample size of the smaller group (cases with non-mild fibrosis) included 31 patients. To avoid overfitting the model, the number of variables in the model should not exceed three ($31 \div 10$), according to the rule of 10 events per variable.²⁰ Therefore, one-, two-, or three-variable models were considered for this study. Thus, 20 (C_{20}^1), 190 (C_{20}^2), and 1039 [$(C_{20}^3 - 1)$] models were tested for each type. One was subtracted from 1040 (C_{20}^3) for the three-variable models because the linear equation with a matrix of the three dummy variables was mathematically unsolvable; therefore, this model was excluded. Thus, there may be 20 univariate, 190 bivariate, and 1039 tri-variate models.

Akaike's information criterion (AIC, for comparison of different models and determining which one is the best for the data; lower AIC scores are better) was used as the index for evaluating the goodness-of-fit of the models.²¹ The models with the best goodness-of-fit (minimum AIC score) in three possible combinations were selected as Models 1, 2, and 3 using the sweeping method, which sweeps all possible combinations of variables to select the optimum model for each type of model, and the model with the lowest AIC score was selected. This sweeping method guaranteed that all possible variable combinations were assessed; otherwise, some combinations of variables might be neglected, and considerable overestimation of regression coefficients might occur for the selected predictors when using the traditional backward stepwise selection method.²²

Univariate and multivariate logistic regression analyses were used to establish the models. The area under the receiver operating characteristics

(ROC) curve (AUC) analysis was used to evaluate the discrimination performance of the models in the training cohort.

Validation of the diagnostic models and nomogram construction

ROC curve analysis was used to evaluate the discrimination performance of models in test cohorts 1 and 2. The DeLong test was then applied for performance comparison between the training and test cohorts of each model.²³

To evaluate the clinical usefulness of these models in test cohorts, decision curve analysis (DCA), an appropriate approach for the evaluation of multiple diagnostic strategies with the advantages of other common methods, was implemented by quantifying the net benefits for a range of threshold probabilities.²⁴

The discrimination performance and clinical practicability of the three models were comprehensively evaluated, and the optimal model was selected for nomogram construction.

Statistical analysis

All statistical analyses in the present study were conducted using SPSS (Version 20.0, International Business Machines Corporation, Armonk, NY, USA) and R software (version 3.5.1, <http://www.Rproject.org>). The Shapiro–Wilk test was used to test whether the measurement data were normally distributed. Student's *t* test was used for those with a normal distribution, and the results are expressed as mean ± standard deviation; otherwise, the Mann–Whitney *U* test was used, and the results are expressed as the median (upper quartile, lower quartile). Categorical variables are expressed as percentages and frequencies. Comparisons of categorical variables between the training and total test cohorts were performed using the Chi-squared test or Fisher's exact test. All statistical tests were two-sided and the threshold probability (*p*) of statistical significance was set at 0.05.

Results

Patients' characteristics

Only specimens with the most pronounced stricture and/or the thickest intestinal wall in each

patient were recruited. A total of 44 intestinal segments with non-mild fibrosis and 130 segments with moderate-to-severe fibrosis were included. The clinical data, pathological fibrosis scores, and selected CTE findings in the training and test cohorts are shown in Table 2. Except for the pathological fibrosis score and CTE findings, we observed no significant statistical difference in other parameters between the training and total test cohorts (all *p* > 0.05).

Valuable variables confirmation

The AIC values for each type of model are shown in Figure 2(a). Models with the best goodness-of-fit (namely the minimum AIC score) of 93.84 for univariate model, 92.24 for bivariate model, and 91.14 for tri-variate model were selected. The corresponding variable combinations in each model type were Model 1 (MCFI), Model 2 (mesenteric oedema and MCFI), and Model 3 (mesenteric oedema, MCFI, and disease duration). There were moderate to good intra-/inter-observer consistencies for the evaluation of MCFI, mesenteric oedema, mesenteric effusion, comb sign, and fibrofatty proliferation score ($\kappa = 0.777–0.863$, all *p* < 0.001).

Development and validation of the diagnostic models

The univariate or multivariate logistic regression analysis formulas of Models 1, 2, and 3 are as follows:

$$\text{Model 1: Logit } P = -2.655 + 0.884 \times \text{MCFI},$$

$$\text{Model 2: Logit } P = -3.030 + 0.787 \times \text{MCFI} + 0.638 \times \text{mesenteric oedema},$$

$$\text{Model 3: Logit } P = -3.734 + 0.847 \times \text{MCFI} + 0.691 \times \text{mesenteric oedema} + 0.008 \times \text{disease duration}.$$

The AUCs of Models 1, 2, and 3 for the training and test cohorts are presented in Table 3. The AUCs of Model 1 in the training cohort and test cohorts 1 and 2 were 0.799 (*p* < 0.001), 0.859 (*p* = 0.001), and 0.693 (*p* = 0.264), respectively; the AUCs of Model 2 were 0.851 (*p* < 0.001), 0.833 (*p* = 0.001), and 0.757 (*p* = 0.138), respectively; and the AUCs of Model 3 were 0.832 (*p* < 0.001), 0.821 (*p* = 0.004), and 0.850 (*p* = 0.043), respectively [Figure 2(b)–(d)]. The DeLong test showed no significant difference in

Table 2. Characteristics of patients with CD in training and test cohorts.

	Test cohort					<i>p</i> *
	Training cohort	Total test cohort (<i>n</i> =83)	Test cohort 1	Test cohort 2		
	Centre 1# (<i>n</i> =91)		Centre 1# (<i>n</i> =30)	Centre 2# (<i>n</i> =35)	Centre 3# (<i>n</i> =18)	
Age [^] , years	31.92 ± 10.68	31 [26, 39]	29.50 [23, 39]	31.77 ± 10.29	35.5 [28.50, 39.50]	0.593
Gender, <i>n</i> (male/female)	66/25	59/24	21/9	25/10	13/5	0.833
Disease duration, months	36 [12, 65]	48 [12, 72]	48 [12, 72]	57 [29, 96]	18 [7.50, 39]	0.316
Time interval between CTE and surgery, days	14.5 [10, 29.25]	14 [10, 25]	23 [11.75, 48.25]	14 [11, 22]	10 [6.75, 14.25]	0.400
Smoking, <i>n</i> (%)	17 (18.68%)	15 (18.07%)	7 (23.33%)	1 (2.86%)	7 (38.89%)	0.918
History of preoperative therapies, <i>n</i> (%)						
Biologics	15 (16.48%)	15 (18.07%)	5 (16.67%)	10 (28.57%)	0	0.782
Corticosteroids	10 (10.99%)	17 (20.48%)	6 (20%)	7 (20%)	4 (22.22%)	0.094
Immunomodulator	29 (31.87%)	48 (57.83%)	21 (70%)	18 (51.43%)	9 (50%)	1.000
Pathological fibrosis score, <i>n</i> (non-mild/moderate-severe)	31/60	13/70	10/20	2/33	1/17	0.005
Mesenteric oedema, <i>n</i> (%)						
None	25 (27.47%)	11 (13.25%)	5 (16.67%)	6 (17.14%)	0	0.038
Mild	26 (28.57%)	35 (42.16%)	11 (36.67%)	20 (57.14%)	4 (22.22%)	
Moderate-to-severe	40 (43.95%)	37 (44.57%)	14 (46.67%)	9 (25.71%)	14 (77.78%)	
MCFI, median (IQR)	4 [3, 6]	3 [2, 4]	3 [2, 6]	4 [3, 5]	2.5 ± 1.20	0.008
1	2 (2.20%)	6 (7.23%)	1 (3.33%)	1 (2.86%)	4 (22.22%)	
2	18 (19.78%)	22 (26.51%)	8 (26.67%)	8 (22.86%)	6 (33.33%)	
3	10 (10.99%)	21 (25.30%)	8 (26.67%)	9 (25.71%)	4 (22.22%)	
4	31 (34.07%)	18 (21.69%)	5 (16.67%)	10 (28.57%)	3 (16.67%)	
5	5 (5.49%)	4 (4.82%)	0	3 (8.57%)	1 (5.56%)	
6	21 (23.08%)	12 (14.46%)	7 (23.33%)	5 (14.29%)	0	
7	4 (4.40%)	2 (2.41%)	1 (3.33%)	1 (2.86%)	0	
8	0	1 (1.20%)	0	1 (2.86%)	0	

#Centre 1, The First Affiliated Hospital of Sun Yat-Sen University; Centre 2, The Sixth Affiliated Hospital of Sun Yat-Sen University; Centre 3, Nanfang Hospital of Southern Medical University.
*Comparison of the differences between the training and total test cohorts.
[^]The results are expressed as mean ± standard deviation or median (upper quartile, lower quartile) depending on whether the data fit a normal distribution.
CD, Crohn's disease; CTE, computed tomography enterography; IQR, interquartile range; MCFI, mesenteric creeping fat index.

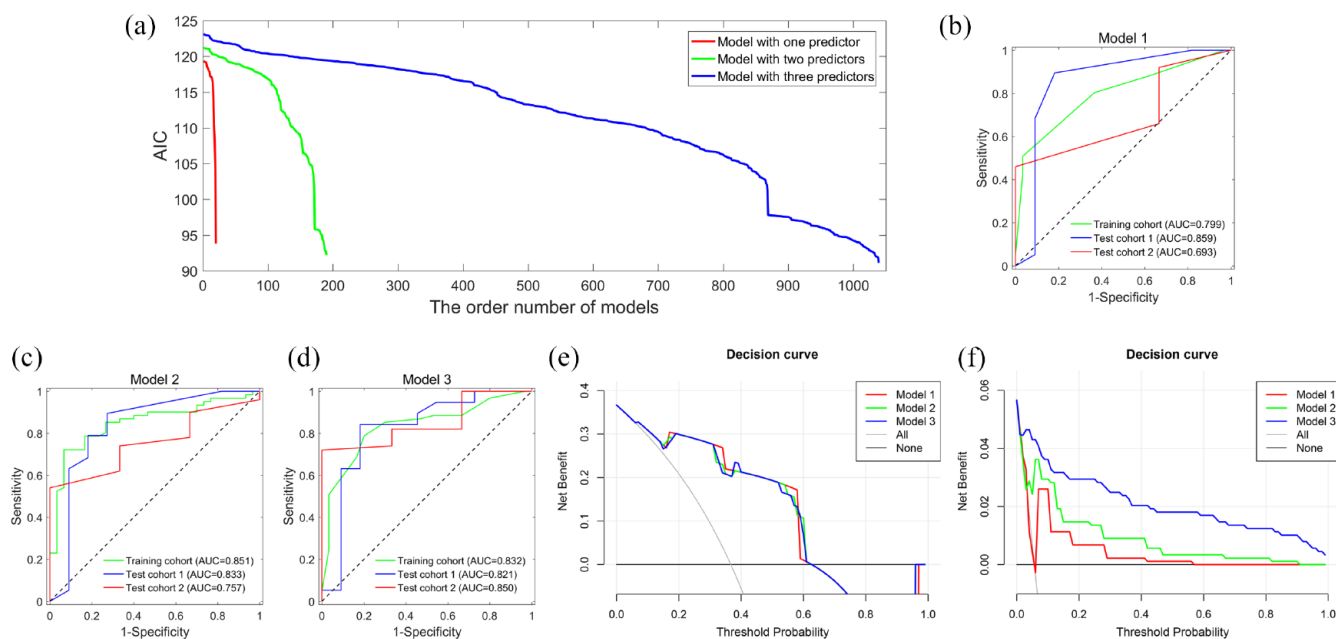


Figure 2. The screening process of models and the diagnostic performances of the optimum models in one predictor, two predictors, and three predictors sets. Image (a) shows the AIC scores of the models with one variable, two variables, and three variables sets, respectively. The red, green, and blue solid lines shown in image (a) represent the AIC scores of 20 univariate, 190 bivariate, and 1039 tri-variate models, respectively. The lowest point of each line indicates that the AIC value in this set is the smallest, corresponding to the optimal model of each set, which is Model 1, 2, or 3 separately. Images (b–d) show the receiver operating characteristic curves of Model 1 (b), which includes MCFI only; and Model 2 (c), which includes mesenteric oedema and MCFI; and Model 3 (d), which includes mesenteric oedema, MCFI, and disease duration. The green, blue, and red lines shown in images (b–d) represent the training cohort, test cohort 1, and test cohort 2, respectively. Images (e) and (f) show the decision curves of Models 1, 2, and 3 in test cohort 1 (e) and test cohort 2 (f). The red, green, and blue solid lines shown in images (e) and (f) represent the Models 1–3, separately.

Model 1 (MCFI), Model 2 (mesenteric oedema and MCFI), and Model 3 (mesenteric oedema, MCFI, and disease duration).

AIC, Akaike's information criterion; AUC, area under the receiver operating characteristic curve; MCFI, mesenteric creeping fat index.

the diagnostic performance between the training and total test cohorts in each model (all $p > 0.05$). Compared to Models 1 and 2, only Model 3 showed robust and satisfactory AUCs for diagnosing bowel fibrosis in all cohorts.

The DCA curves for the three models in the test cohorts are presented in Figure 2(e) and (f). It was visually inferred from graphs that the optimum cut-off probabilities of the three models were all located in the range of 'useful' threshold probabilities (between 45% and 93%). Compared to Models 1 and 2, Model 3 showed the highest net clinical benefit in test cohort 2, although this advantage was not evident in test cohort 1.

Nomogram construction

Considering the above-mentioned overall excellent diagnostic performance of Model 3, it was selected

as the optimal model for differentiating between non-mild and moderate-to-severe fibrotic intestinal strictures in patients with CD. Subsequently, the nomogram of Model 3 was developed for better clinical use. Cases for distinguishing affected bowel walls with non-mild or moderate-to-severe fibrosis in patients with CD using this nomogram are shown in Figure 3. The three parameters in this model corresponded to one score, and the sum of the three scores was the total score for each case. This total score corresponded to the probability of the affected intestinal wall with moderate-to-severe fibrosis predicted by Model 3.

Discussion

This study showed that Model 3 (MCFI, mesenteric oedema, and disease duration) had the most satisfactory clinical practicability and optimal performance for differentiating between non-mild and

Table 3. The AUCs of the three selected models in training and test cohorts.

	Model 1			Model 2			Model 3		
	Training cohort	Test cohort 1	Test cohort 2	Training cohort	Test cohort 1	Test cohort 2	Training cohort	Test cohort 1	Test cohort 2
AUC	0.799	0.859	0.693	0.851	0.833	0.757	0.832	0.821	0.850
95% CI	0.708–0.890	0.686–1.000	0.451–0.935	0.769–0.933	0.655–1.000	0.567–0.946	0.744–0.920	0.643–0.998	0.700–1.000
<i>p</i>	<0.001	0.001	0.264	<0.001	0.003	0.138	<0.001	0.004	0.043

Model 1 (MCFI), Model 2 (mesenteric oedema and MCFI), and Model 3 (mesenteric oedema, MCFI, and disease duration).
AUC, area under the receiver operating characteristics curve; 95% CI, 95% confidence interval; MCFI, mesenteric creeping fat index.

moderate-to-severe fibrotic intestinal strictures in patients with CD compared with the other two models. Moreover, the diagnostic performance of Model 3 was stable among the three multicentre cohorts. Thus, we constructed a nomogram for Model 3 to visualize and quantify intestinal fibrosis, which made it feasible for wide and easy use in clinical practice. Notably, in the many candidate CTE features, only the mesenteric signs, rather than the bowel signs, were selected in the models, suggesting that information from the mesentery (such as CF) may be of greater diagnostic value for the evaluation of intestinal fibrosis.

Compared with Models 1 and 2, Model 3 showed a similar or superior diagnostic performance for the evaluation of intestinal fibrosis in patients with CD in the training cohort and the two test cohorts, and Model 3 also showed an equivalent or higher net clinical benefit for the two test cohorts. The better diagnostic performance of Model 3 might be because it was a comprehensive model that included not only more imaging features but also a clinical marker. Hence, more information can be captured to address this issue. It was widely accepted that CTE findings do not correlate with bowel fibrosis in CD.⁵ In a paediatric CD study, the diagnostic accuracy of CTE for evaluating intestinal fibrosis was only 55.6%, which was far less effective than that of Model 3.²⁵ One of the possible reasons for the low accuracy of this prior study was that it mainly focused on the intestinal features and did not pay close attention to the mesentery. Conventional CTE bowel features cannot satisfactorily characterize bowel fibrosis unless novel image analysis methods are employed, such as radiomics or deep learning.^{13,26} Contrarily, our study attached great importance to abnormalities of the mesentery. We analysed not only many conventional mesenteric findings,

such as the comb sign and mesenteric oedema, but also the degree of CF wrapping around the inflamed gut (i.e. MCFI). This new analytical perspective gave us an encouraging result. In order to clinically generalize Model 3, we constructed a nomogram for Model 3. As shown in Figure 3(a), the three parameters corresponded to one score, and the sum of these scores was 81.25, with a prediction probability of the affected intestinal wall with moderate-to-severe fibrosis of 78%. These three parameters can be easily obtained from routine CTE images or medical history of patients and the prediction result was consistent with the pathological finding, indicating its feasibility and high efficacy.

Mesenteric adipose tissue, particularly CF, has recently been considered to play an important role in the pathogenesis of bowel fibrosis in CD.²⁷ Gastrointestinal surgeons have often observed that bowel fibrotic strictures and CF are topographically coupled in CD.²⁸ Significant abnormalities were also found in the mesenchymal tissue of CF, which was similar to the mesenchymal lesions in the submucosa of intestinal walls in patients with CD.^{29,30} The CF connective tissue was continuous with the serosa of the diseased intestinal wall and extended into its longitudinal muscle layer.²⁸ Furthermore, the mesentery and intestine may function synergistically, with the mesentery acting as a connective tissue between different parts of the intestine.³¹ The above studies suggest that there is a direct interaction between CF and intestinal lesions in CD and can explain why CF (i.e. MCFI) has the potential to characterize intestinal fibrosis. In our previous study, MCFI was reported to be associated with intestinal collagen fibre deposition and smooth muscle hyperplasia/hypertrophy.¹⁰ The higher the MCFI, that is, the wider the range of CF

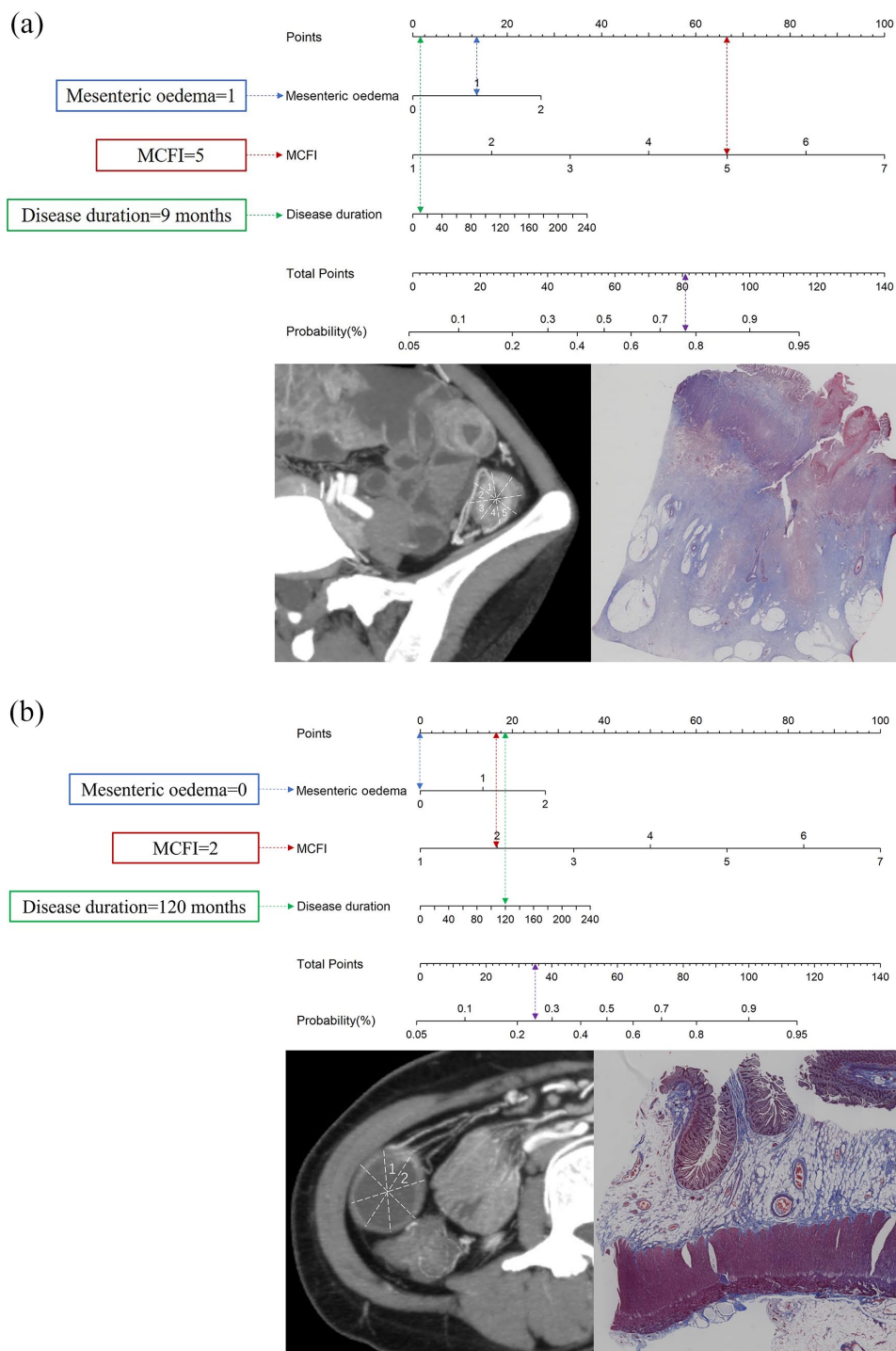


Figure 3. Nomogram for Model 3. The total points of mesenteric oedema, MCFI, and disease duration score of the affected bowel segment corresponding to its prediction probability of moderate-to-severe fibrosis are shown. Image (a) shows a case with mild mesenteric oedema, five eighths of mesenteric vessels surrounding the affected intestine, and 9 months of disease duration, with a total score of 81.25. The probability of an intestinal wall with moderate-to-severe fibrosis predicted by Model 3 was 0.78. The image on the lower right shows Masson's trichrome staining (0.31 \times) of the intestinal wall with a pathological fibrosis score of 4, indicating moderate-to-severe fibrosis. Image (b) shows a case with no mesenteric oedema, two eighths of mesenteric vessels surrounding the affected intestine, and 120 months of disease duration, with a total score of 35. The probability of the intestinal wall with moderate-to-severe fibrosis predicted by Model 3 was 0.25. The image on the lower right shows Masson's trichrome staining (0.66 \times) of the intestinal wall with a pathological fibrosis score of 2, indicating non-mild fibrosis. MCFI, mesenteric creeping fat index.

wrapping the affected bowel, the higher the risk of moderate-to-severe fibrotic stenosis.¹⁰ The efficacy of the MCFI for the diagnosis of bowel fibrosis in the present study was consistent with that of a previous study.¹⁰ Mesenteric oedema is a common imaging feature of the mesentery in CD that reflects severe intestinal inflammation or might be used as a predictor for bowel resection.^{32,33} Given that intestinal inflammation always coexists with bowel fibrosis, especially in CD patients with long disease courses, mesenteric oedema and disease course might be able to indirectly suggest the presence of moderate-to-severe intestinal fibrosis.^{12,25}

Our study had some limitations. First, because surgical specimens were used as the reference standard for more severe disease, only a small sample of intestinal segments with non-mild fibrosis were enrolled in this study. The efficacy of Model 3 in assessing intestinal fibrosis at an earlier stage of CD needs to be further clarified. Second, this study was retrospective, and future multicentre validation on prospective cohorts with a large sample size would enhance its conclusion.

In conclusion, the nomogram of Model 3, which combined mesenteric abnormalities on CTE with a clinical marker, was highly interpretable for the differentiation of non-mild and moderate-to-severe fibrotic intestinal strictures, providing valuable and intuitive information for tailored treatment in patients with CD.

Declarations

Ethics approval and consent to participate

This retrospective study was approved by the Ethics Committee of the First Affiliated Hospital of Sun Yat-sen University (No. 2020[177]), and there was informed consent exemption for all patients.

Consent for publication

All authors approved the final manuscript and the submission to this journal.

Author contributions

Jixin Meng: Data curation; Project administration; Writing – original draft.

Yitao Mao: Data curation; Project administration; Writing – original draft.

Jie Zhou: Data curation; Project administration; Writing – original draft.

Zhao Chen: Data curation; Formal analysis.

Siyun Huang: Data curation; Formal analysis.

Yangdi Wang: Data curation; Formal analysis.

Li Huang: Data curation; Formal analysis.

Ruonan Zhang: Investigation.

Xiaodi Shen: Investigation.

Wen Lv: Investigation.

Juxiong Xiao: Investigation.

Ziyin Ye: Formal analysis.

Zhihui Chen: Formal analysis.

Ren Mao: Supervision.

Canhui Sun: Supervision.

Ziping Li: Supervision.

Shi-Ting Feng: Supervision.

Shaochun Lin: Conceptualization; Methodology; Writing – review & editing.

Xuehua Li: Conceptualization; Methodology; Writing – review & editing.

Acknowledgements

None.

Funding

The authors disclosed receipt of the following financial support for the research, authorship, and/or publication of this article: This study was supported by the National Natural Science Foundation of China (grant numbers 82070680, 81870451, and 82072002), Natural Science Foundation of Hunan Province (2022JJ30794) and Changsha Municipal Natural Science Foundation (kq2202126). The funders had no role in the study design, data collection, data analysis, data interpretation, or writing of the report.

Competing interests

The authors declare that there is no conflict of interest.

Availability of data and materials

The datasets used and analysed during the current study are available from the corresponding author on reasonable request.

ORCID iDs

Jixin Meng  <https://orcid.org/0000-0002-5698-2600>

Xuehua Li  <https://orcid.org/0000-0002-7476-2644>

Supplemental material

Supplemental material for this article is available online.

References

- Latella G, Di Gregorio J, Flati V, *et al.* Mechanisms of initiation and progression of intestinal fibrosis in IBD. *Scand J Gastroenterol* 2015; 50: 53–65.
- Bettenworth D, Bokemeyer A, Baker M, *et al.* Assessment of Crohn's disease-associated small bowel strictures and fibrosis on cross-sectional imaging: a systematic review. *Gut* 2019; 68: 1115–1126.
- Rieder F, Bettenworth D, Ma C, *et al.* An expert consensus to standardise definitions, diagnosis and treatment targets for anti-fibrotic stricture therapies in Crohn's disease. *Aliment Pharmacol Ther* 2018; 48: 347–357.
- Panes J, Bouhnik Y, Reinisch W, *et al.* Imaging techniques for assessment of inflammatory bowel disease: joint ECCO and ESGAR evidence-based consensus guidelines. *J Crohns Colitis* 2013; 7: 556–585.
- Adler J, Punglia DR, Dillman JR, *et al.* Computed tomography enterography findings correlate with tissue inflammation, not fibrosis in resected small bowel Crohn's disease. *Inflamm Bowel Dis* 2012; 18: 849–856.
- Kredel LI and Siegmund B. Adipose-tissue and intestinal inflammation - visceral obesity and creeping fat. *Front Immunol* 2014; 5: 462.
- Mao R, Kurada S, Gordon IO, *et al.* The mesenteric fat and intestinal muscle interface: creeping fat influencing stricture formation in Crohn's disease. *Inflamm Bowel Dis* 2019; 25: 421–426.
- Sheehan AL, Warren BF, Gear MW, *et al.* Fat-wrapping in Crohn's disease: pathological basis and relevance to surgical practice. *Br J Surg* 1992; 79: 955–958.
- Westcott ED, Mattacks CA, Windsor AC, *et al.* Perinodal adipose tissue and fatty acid composition of lymphoid tissues in patients with and without Crohn's disease and their implications for the etiology and treatment of CD. *Ann N Y Acad Sci* 2006; 1072: 395–400.
- Li XH, Feng ST, Cao QH, *et al.* Degree of creeping fat assessed by computed tomography enterography is associated with intestinal fibrotic stricture in patients with Crohn's disease: a potentially novel mesenteric creeping fat index. *J Crohns Colitis* 2021; 15: 1161–1173.
- Catalano OA, Gee MS, Nicolai E, *et al.* Evaluation of quantitative PET/MR enterography biomarkers for discrimination of inflammatory strictures from fibrotic strictures in Crohn's disease. *Radiology* 2016; 278: 792–800.
- Rimola J, Planell N, Rodríguez S, *et al.* Characterization of inflammation and fibrosis in Crohn's disease lesions by magnetic resonance imaging. *Am J Gastroenterol* 2015; 110: 432–440.
- Li XH, Liang D, Meng JX, *et al.* Development and validation of a novel computed-tomography enterography radiomic approach for characterization of intestinal fibrosis in Crohn's disease. *Gastroenterology* 2021; 160: 2303–2316. e11.
- Sakurai T, Katsuno T, Saito K, *et al.* Mesenteric findings of CT enterography are well correlated with the endoscopic severity of Crohn's disease. *Eur J Radiol* 2017; 89: 242–248.
- Liu YB, Liang CH, Zhang ZL, *et al.* Crohn disease of small bowel: multidetector row CT with CT enteroclysis, dynamic contrast enhancement, CT angiography, and 3D imaging. *Abdom Imaging* 2006; 31: 668–674.
- Silverman PM, Baker ME, Cooper C, *et al.* Computed tomography of mesenteric disease. *Radiographics* 1987; 7: 309–320.
- Chopra S, Dodd GD, Chintapalli KN, *et al.* Mesenteric, omental, and retroperitoneal edema in cirrhosis: frequency and spectrum of CT findings. *Radiology* 1999; 211: 737–742.
- Radmard AR, Eftekhar Vaghefi R, Montazeri SA, *et al.* Mesenteric lymph nodes in MR enterography: are they reliable followers of bowel in active Crohn's disease? *Eur Radiol* 2018; 28: 4429–4437.
- Erhayiem B, Dhingsa R, Hawkey CJ, *et al.* Ratio of visceral to subcutaneous fat area is a biomarker of complicated Crohn's disease. *Clin Gastroenterol Hepatol* 2011; 9: 684–687. e1.
- Riley RD, Ensor J, Snell KIE, *et al.* Calculating the sample size required for developing a clinical prediction model. *BMJ* 2020; 368: m441.

21. Pan W. Akaike's information criterion in generalized estimating equations. *Biometrics* 2001; 57: 120–125.
22. Steyerberg EW, Eijkemans MJ and Habbema JD. Stepwise selection in small data sets: a simulation study of bias in logistic regression analysis. *J Clin Epidemiol* 1999; 52: 935–942.
23. DeLong ER, DeLong DM and Clarke-Pearson DL. Comparing the areas under two or more correlated receiver operating characteristic curves: a nonparametric approach. *Biometrics* 1988; 44: 837–845.
24. Vickers AJ and Elkin EB. Decision curve analysis: a novel method for evaluating prediction models. *Med Decis Making* 2006; 26: 565–74.
25. Quencer KB, Nimkin K, Mino-Kenudson M, *et al.* Detecting active inflammation and fibrosis in pediatric Crohn's disease: prospective evaluation of MR-E and CT-E. *Abdom Imaging* 2013; 38: 705–713.
26. Meng JX, Luo ZX, Chen Z, *et al.* Intestinal fibrosis classification in patients with Crohn's disease using CT enterography-based deep learning: comparisons with radiomics and radiologists. *Eur Radiol*. Epub ahead of print 26 May 2022. DOI: 10.1007/s00330-022-08842-z.
27. Wang J, Lin S, Brown JM, *et al.* Novel mechanisms and clinical trial endpoints in intestinal fibrosis. *Immunol Rev* 2021; 302: 211–227.
28. Coffey CJ, Kiernan MG, Sahebally SM, *et al.* Inclusion of the mesentery in ileocolic resection for Crohn's disease is associated with reduced surgical recurrence. *J Crohns Colitis* 2018; 12: 1139–1150.
29. Coffey JC, O'Leary DP, Kiernan MG, *et al.* The mesentery in Crohn's disease: friend or foe? *Curr Opin Gastroenterol* 2016; 32: 267–273.
30. Kredel L, Batra A and Siegmund B. Role of fat and adipokines in intestinal inflammation. *Curr Opin Gastroenterol* 2014; 30: 559–565.
31. Suau R, Pardina E, Domènech E, *et al.* The complex relationship between microbiota, immune response and creeping fat in Crohn's-disease. *J Crohns Colitis* 2022; 16: 472–489.
32. Rosenbaum DG, Conrad MA, Biko DM, *et al.* Ultrasound and MRI predictors of surgical bowel resection in pediatric Crohn disease. *Pediatr Radiol* 2017; 47: 55–64.
33. Dillman JR, Smith EA, Sanchez RJ, *et al.* Pediatric small bowel Crohn disease: correlation of US and MR enterography. *Radiographics* 2015; 35: 835–848.

Visit SAGE journals online
[journals.sagepub.com/
home/tag](https://journals.sagepub.com/home/tag)

 SAGE journals